Raman-spectroscopic study of lanthanide trifluorides with the β-YF_3 structure

2004 J. Phys.: Condens. Matter 16 3207

(http://iopscience.iop.org/0953-8984/16/18/021)

INSTITUTE OF PHYSICS PUBLISHING JOURNAL OF PHYSICS: CONDENSED MATTER

J. Phys.: Condens. Matter **16** (2004) 3207–3218 PII: S0953-8984(04)71814-7

Raman-spectroscopic study of lanthanide trifluorides with the β-YF_3 structure

M M Lage[1], A Righi[1], F M Matinaga[1], J-Y Gesland[2] and R L Moreira[1,3]

[1] Departamento de Física, ICEx, UFMG, CP 702, 30123-970 Belo Horizonte (MG), Brazil
[2] Université du Maine-Cristallogénèse, UMR 6087, 72085 Le Mans cedex9, France

E-mail: bmoreira@fisica.ufmg.br

Received 10 November 2003
Published 23 April 2004
Online at stacks.iop.org/JPhysCM/16/3207
DOI: 10.1088/0953-8984/16/18/021

Abstract

We have performed polarized Raman scattering measurements on several Czochralski-grown lanthanide trifluoride (LnF_3) crystals presenting the β-YF_3 structure (space group: $Pnma$). The phonon mode assignments for the DyF_3 and LuF_3 spectra are given for the first time. Besides this, the Raman spectra of TbF_3, ErF_3 and YbF_3 complete and extend previous studies on these materials. The vibrational modes of LnF_3 compounds are then correlated with those of the archetype β-YF_3 crystal. The totally symmetrical fundamentals present a strong dependence on the scattering geometry, similar to what is shown by molecular crystals with weakly interacting molecules. Most of the Raman features are well behaved with the lanthanide ion substitution. Although the observed modes always involve all ions, it was possible to discern modes that are dominated by the motion of either the lanthanide or the fluorine ions. The intensity of some low frequency modes has proved to be quite dependent on the orthorhombic distortion of the quasi-hexagonal structure.

1. Introduction

Fluoride crystalline materials are commonly studied owing to their applications in the fields of solid state lasers and scintillators. Indeed, their good optical properties beside their low non-radiative emissions (mainly because of the low cut-off phonon frequencies) make these materials good host matrices for visible or infrared light emission and other optical applications [1]. Among these crystals, $LiYF_4$ (YLF) is the most frequently studied and used one, with several laser emission lines, depending on the choice of the active centre (a doping cation in the yttrium site), that can be a lanthanide ion (Nd^{3+}, Eu^{3+}, ...) or even an actinide ion (U^{3+}) [2–5]. Other optically transparent fluoride crystals containing lanthanide ions could

[3] Author to whom any correspondence should be addressed.

also emerge as good candidates for those applications, since they can easily be doped with different trivalent rare earth or transition metals. For that reason, renewed interest has arisen in some old or new systems, such as *scheelite* crystals (which are isomorphous with YLF), like $LiLnF_4$ (Ln = Ho, Er, Tm and Yb) and Li_2CaHfF_8, whose phonon spectra were determined only recently [6–9], and some lanthanide trifluorides (LnF_3), since Kollia *et al* showed that yttrium fluoride (YF_3) crystal could be a laser material [10].

At room temperature, YF_3 belongs to the orthorhombic $Pnma$ (D_{2h}^{16}) space group with four formulae per unit cell [11, 12]. This structure is known as β-YF_3 and is stable up to 1350 K. At this temperature, the crystal undergoes a structural phase transition (SPT) to a trigonal $P\overline{3}m1$ symmetry (D_{3d}^{3}, with one formula per unit cell), so-called α-YF_3 [13–17]. Due to the reconstructive nature of this SPT and to the strong unit cell mismatching between the two structures, the crystal breaks completely during the transition. This explains why optical studies on this material are relatively recent, as compared to structural determinations. In fact, it was only recently that we obtained large and good optical quality Czochralski-pulled YF_3 crystals, by crystallizing the material directly in its β-phase, below the SPT temperature [18]. The same method has also been successfully applied to other LnF_3 compounds that present the same destructive SPT, leading to the possibility of studying these materials too.

The lower atomic number LnF_3 crystals (Z from 57 to 60, i.e. La, Ce, Pr and Nd) crystallize in the trigonal *tysonite* $P\overline{3}c1$ structure (D_{3d}^{4}, with six formulae per unit cell), which is stable down to room temperature [19–21]. Thus, large crystals of these materials can be easily obtained, so their optical phonons were determined concomitantly with their structure [22]. For all LnF_3 compounds with Z ranging from 62 to 71 (from Sm to Lu) the room temperature structure is the same as that of β-YF_3. Nevertheless, these crystals do not have the same temperature behaviour and growth conditions because they show different high temperature SPT sequences, as follows [15–17, 23, 24]:

(i) for Ln = Sm, Eu and Gd ($Z = 62$, 63 and 64, respectively), the crystals undergo two SPT on heating: a destructive SPT (with crystal cracking) to the LaF_3 structure and, then, a second one to a hexagonal $P6_3/mmc$ structure (D_{6h}^{4}, with two formulae per unit cell);

(ii) for Ln = Tb, Dy and Ho ($Z = 65$, 66 and 67, respectively), the room temperature phase is stable up to the melting point;

(iii) for Ln = Er, Tm, Yb and Lu (increasing Z from 68 to 71), the crystals behave like YF_3, i.e. they undergo only one destructive SPT to the α-YF_3 structure.

While LaF_3-type crystals are not interesting as luminescent host matrices, the β-YF_3 ones could be promising for that purpose. The lower coordination number [24], the shorter nearest-neighbour distances and the larger fine-interaction parameter for the latest structure account for this different behaviour [25, 26]. In fact, the fine-interaction parameter for Gd^{3+} in YF_3 and LuF_3 is of the same order as that presented by $LiYF_4$ and twice as large as for LaF_3 [25–28]. It is noteworthy that the laser threshold decreases with the increasing of that parameter, which can explain the observed laser behaviour of YF_3 [10]. The same holds also for other optical luminescent applications, such as in scintillators.

In order to contribute to the knowledge of the optical behaviour of β-YF_3-type crystals we carried out Raman scattering measurements on several Czochralski-grown crystals. In this work we present the phonon mode assignment for DyF_3 and LuF_3, whose spectra are, at our knowledge, obtained for the first time. Also, our Raman spectra of TbF_3, ErF_3 and YbF_3 complete and extend previous studies on these crystals [23, 29, 30]. The vibrational modes of LnF_3 compounds are then correlated with those of the archetype β-YF_3 crystal.

Table 1. Ln^{3+} ionic radii for the coordination number equal to nine (from [34]), lattice parameters, unit cell volumes and the orthorhombic elastic distortions of LnF_3 (and YF_3) in the β-YF_3 structure. The crystallographic parameters (at room temperature) were taken from the JCPDS-ICDD database.

Lanthanide ion	Lu^{3+}	Yb^{3+}	Er^{3+}	Y^{3+}	Dy^{3+}	Tb^{3+}
Ionic radius (Å)	1.032	1.042	1.062	1.075	1.083	1.095
a (Å)	6.151	6.216	6.349	6.365	6.458	6.508
b (Å)	6.761	6.786	6.843	6.857	6.908	6.948
c (Å)	4.469	4.432	4.382	4.392	4.381	4.391
V (Å^3)	185.83	186.94	190.38	191.67	195.44	198.54
ε (deg)	6.022	5.506	4.623	4.617	4.160	4.014

2. Experimental procedures

Optical quality YF_3 and LnF_3 (Ln = Tb, Dy, Er, Yb and Lu) single crystals with around 2 cm^3 volume were pulled by the Czochralski technique, from mixtures containing 20%–40% of LiF added to LnF_3. The equilibrium diagrams of these mixtures show that pure LnF_3 crystals crystallize directly from the melt in the orthorhombic β-YF_3 structure (due to the melting point depression) [18, 31]. The crystals were pulled in the (010) direction, which is revealed to be perpendicular to an easy cleavage plane. They also presented clear natural faces, indicating different growth rates according to the (100) and (001) directions. These faces, together with the structural birefringence in the *ac* plane, helped us to orient the crystals before cutting. All the samples were then oriented and cut according their crystallographic axes ($3 \times 2 \times 3$ mm^3 size); after this they were optically polished with 0.25 μm diamond paste (except the cleaved *ac* surfaces). DyF_3 and ErF_3 crystals present respectively light citrine and pink colours, while all the other crystals are completely transparent.

The Raman spectra of the light scattered by the crystals were collected in the back-scattering configuration by using a T64000 Jobin-Yvon spectrometer equipped with a LN_2-cooled CCD detector. The 488.1 nm line of a Coherent Radiation argon ion laser (200 mW) has proved to be the better choice as the exciting line for the crystals DyF_3, YbF_3 and LuF_3, avoiding the appearance of additional lines in Raman spectra (due to the luminescence coming from rare earth impurities, as shown in [23]). For the other crystals, better choices were 457.9 nm (50 mW) for ErF_3 and 514.5 nm (250 mW) for YF_3 and TbF_3. The spectral resolution was typically 3 cm^{-1} and the accumulation times were typically 10×40 s. The scattering geometries for the spectra presented in the text and figures follow the usual Porto notation, $A(BC)D$ [32]. All the spectra were previously divided out by the Bose factor [33] and, then, fitted by a sum of Lorentzian lines.

3. Crystalline structure and group theory

As already pointed out, all the crystals studied here exhibit, at room temperature, the β-YF_3 structure, which has an orthorhombic symmetry within the space group $Pnma$ (D_{2h}^{16}), with four molecules per unit cell ($Z = 4$) [12]. The unit cell is a distorted hexagonal LaF_3 lattice, although there is no group-to-subgroup relationship between these two structures (the relationship between them is given by the common D_{6h} supergroup). The lattice parameters (taken from the JCPDS-ICDD database), beside the lanthanide ionic radii, unit cell volume and the orthorhombic distortion angle ε for each crystal are presented in table 1. The ionic radii were taken from [34], taking into account that the rare earth ions in the orthorhombic

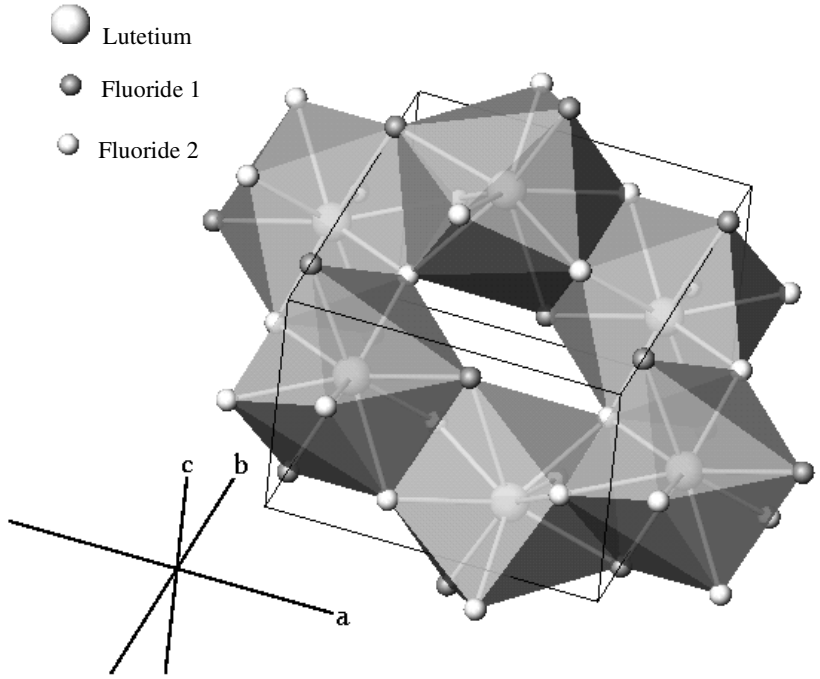

Figure 1. The six-tricapped-prism cycle in the orthorhombic β-YF_3 crystalline structure.

structure are coordinated by nine fluorine ions [24, 25]. The distortion angle ε is defined here as the difference between the hexagonal in-plane 60° angle and the corresponding angle in the distorted cell, i.e. $\varepsilon = \tan^{-1}[(\sqrt{3}c - a)/(c + \sqrt{3}a)]$, since the orthorhombic b parameter is parallel to the principal axis of the hexagonal cell [24]. The usefulness of this parameter will become clear in the next section.

The crystalline structure of β-YF_3 crystals has usually been described by six-tricapped-prism cycles that overlap each other in the three crystallographic directions [18]. Moreover, for each cycle, four prisms form pairs by sharing faces, while the two other prisms link the pairs through edges. A 3D view of the ring forming this orthorhombic structure is given in figure 1. In order to predict the number and assignment of the vibrational modes for this structure we used the factor group analysis of Rousseau *et al* [35], which only requires knowledge of the space group and Wyckoff positions [36] of each ion in the crystalline unit. In the β-YF_3 structure the fluorine ions occupy two sites with different symmetries. They are called F_1 and F_2, for the ions occupying the Wyckoff sites (4)c or (8)d, respectively (the multiplicities are given in parentheses). The Ln ions occupy also sites with (4)c symmetry. Then, table 2 summarizes the site symmetries and presents the corresponding normal modes at the centre of the Brillouin zone (48 degrees of freedom). The 24 even modes of this centrosymmetrical structure ($7A_g + 5B_{1g} + 7B_{2g} + 5B_{3g}$) are Raman active. Moreover, since all ions are involved in each mode, the use of the projection operators to determine the symmetry coordinates for each mode does not provide much information. We will restrict their use only to helping in the analysis of some modes with anomalous behaviour. Therefore, in order to distinguish and assign the Raman modes, we consider the Raman polarizability tensors for the D_{2h} point

Table 2. Factor group analysis for the LnF_3 crystals with β-YF_3 structure.

Ion	Wyckoff site	Irreducible representations
Ln^{3+}	4c	$2A_g + B_{1g} + 2B_{2g} + B_{3g} + A_u + 2B_{1u} + B_{2u} + 2B_{3u}$
F_1^{-1}	4c	$2A_g + B_{1g} + 2B_{2g} + B_{3g} + A_u + 2B_{1u} + B_{2u} + 2B_{3u}$
F_2^{-1}	8d	$3A_g + 3B_{1g} + 3B_{2g} + 3B_{3g} + 3A_u + 3B_{1u} + 3B_{2u} + 3B_{3u}$
	Total	$7A_g + 5B_{1g} + 7B_{2g} + 5B_{3g} + 5A_u + 7B_{1u} + 5B_{2u} + 7B_{3u}$
	Raman active	$7A_g + 5B_{1g} + 7B_{2g} + 5B_{3g}$

group [33], shown below:

$$A_g \begin{pmatrix} a & \cdot & \cdot \\ \cdot & b & \cdot \\ \cdot & \cdot & c \end{pmatrix}, \qquad B_{1g} \begin{pmatrix} \cdot & d & \cdot \\ d & \cdot & \cdot \\ \cdot & \cdot & \cdot \end{pmatrix}, \qquad B_{2g} \begin{pmatrix} \cdot & \cdot & e \\ \cdot & \cdot & \cdot \\ e & \cdot & \cdot \end{pmatrix} \qquad \text{and}$$

$$B_{3g} \begin{pmatrix} \cdot & \cdot & \\ \cdot & \cdot & f \\ \cdot & f & \cdot \end{pmatrix}.$$

Since the structure has an inversion centre, none of the Raman modes can be polar. In such cases, the Raman bands depend only on the polarization of the incoming and scattered lights (they do not depend on the light beam propagation directions) [33]. Thus, we can choose either classical 90° or back-scattering geometries. In this work, we used the latest geometry, since our experimental set-up has a very good stray light rejection. Then, the Raman polarizability tensors impose quite restrictive selection rules: A_g modes are observed in (aa), (bb) or (cc) polarizations, B_{1g} modes in (ab) polarization, B_{2g} modes in (ac) polarization and B_{3g} in (bc) polarization. Note that only the directions of the light polarizations, within the Porto notation, are required to distinguish the modes.

4. Results and discussions

The Raman spectra of DyF_3 and LuF_3 are presented in figures 2 and 3, for the six back-scattering geometries indicated in the figures. The mode assignments are also indicated in the figures. The peak leakages of the A_g, B_{2g} and B_{3g} modes are indicated by the symbols ●, ▽ and ◊, respectively. In general, the spectra of the two materials show similar numbers of Raman modes and frequencies for each configuration, because the crystals have the same symmetry and very close masses and ionic radii. Nevertheless, only their cross-polarized (ab) and (bc) spectra look really very close. In the other four cases, the Raman peak intensities are different for the two crystals.

Before analysing the origin of the above-mentioned differences in the Raman intensities, let us verify the validity of the group theory predictions for our crystals. Considering the three parallel polarizations together, seven A_g modes were discerned for each crystal, as predicted. Nevertheless, each mode is always relatively intense in two polarizations and weak, or even absent, in the third one (see, for instance, the higher frequency A_g mode, which is practically absent in the (cc) polarization). The same behaviour was observed for the other rare earth (RE) trifluorides studied here (RE = Y, Tb, Er and Yb) and can also be seen in the spectra of [18] and [23], where the authors studied several LnF_3 samples of the same β-YF_3 structure, with 90° scattering geometries. Thus, the observed behaviour is a general property of this system that does not depend on the particular RE ion or on the phonon propagation direction. A similar behaviour was observed for some molecular crystals with weakly interacting molecules,

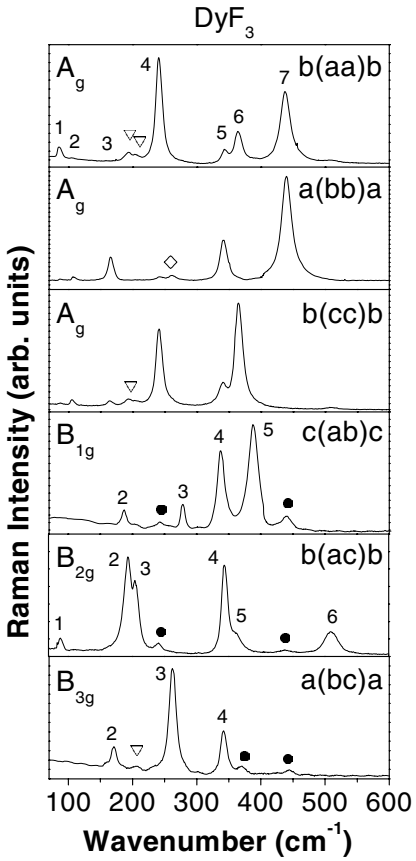

Figure 2. Polarized Raman spectra for the DyF_3 crystal, for six different scattering geometries. The mode assignments and the peak leakages of A_g (●), B_{2g} (▽) and B_{3g} (◇) modes are also indicated.

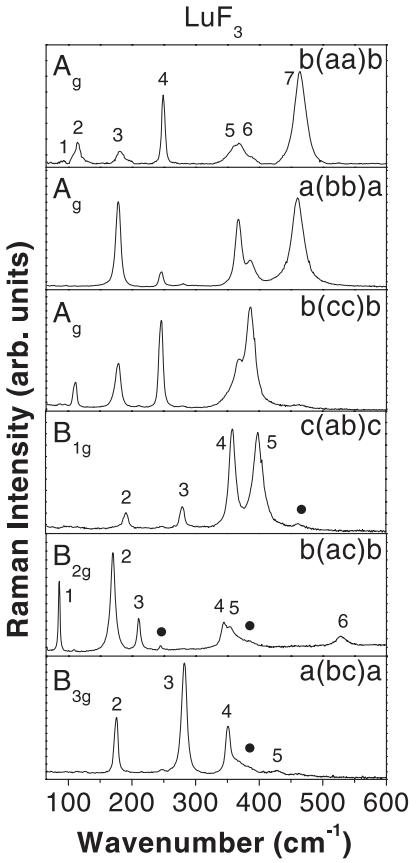

Figure 3. Polarized Raman spectra for the LuF_3 crystal, for the six scattering geometries used. The mode assignments and peak leakage of the intense Ag (●) mode are also indicated in the figure.

where the symmetry rules for the molecules impose some restrictions on the intensity of totally symmetrical Raman lines of the crystal, linked to the particular orientation of these molecules [37]. In the case of the LnF_3, the Ln coordination polyhedra have well defined directions, since the three F_1 ions surrounding the lanthanide ions lie in planes parallel to the crystallographic *ac* plane [25]. Thus, the totally symmetrical vibrations are expected to contribute differently in different polarizations. However, the mathematical description of this feature becomes complicated, because of ambiguities in correlating the intensities of the modes of a cluster-like molecule with those of the crystalline system [37].

The frequencies and linewidths of the Raman modes of all crystals studied here are summarized in table 3. Although some bands are too weak to be observed for some crystals, on the whole, the Raman phonon modes of the β-YF_3 crystals agree very well with the group theory predictions: from the 24 predicted modes only one B_{2g} mode was missing. Also, our assignments are in good agreement with those of [23] (for Ln = Gd, Tb, Er and Yb), but present many differences compared to those of [29] (for Ln = Sm, Tb, Ho and Yb), where the authors used polycrystals (except for TbF_3, which, however, was badly oriented). We observe from table 3 that some low frequency modes have higher frequency for Y ions than for the Ln ones.

Table 3. Assignments of the Raman-active modes obtained (in cm^{-1}) for β-YF_3 and LnF_3 crystals and the respective linewidths (in parentheses, also in cm^{-1}), for increasing atomic number.

Modes	No	Y	Tb	Dy	Er	Yb	Lu
A_g	1	118(8)	86(11)	86(9)	91(15)	93(8)	86(12)
	2	145(6)	107(7)	106(8)	108(10)	110(6)	111(6)
	3	171(9)	160(9)	164(11)	174(12)	178(12)	178(9)
	4	244(11)	241(12)	240(13)	244(12)	247(12)	246(9)
	5	351(14)	336(12)	341(12)	350(14)	363(14)	367(12)
	6	367(11)	360(13)	364(15)	375(16)	385(14)	385(17)
	7	444(21)	432(18)	439(19)	451(19)	455(27)	464(23)
B_{1g}	1	138(10)	125(7)	—	—	—	—
	2	221(10)	185(10)	187(10)	189(13)	191(12)	191(10)
	3	295(9)	274(9)	278(7)	285(12)	283(10)	280(10)
	4	367(11)	331(11)	337(15)	347(16)	356(24)	358(12)
	5	391(12)	381(17)	387(20)	396(19)	401(25)	398(19)
B_{2g}	1	120(9)	89(7)	88(11)	92(7)	89(10)	85(8)
	2	188(8)	196(12)	194(15)	191(15)	180(16)	169(11)
	3	—	207(8)	205(11)	210(11)	214(10)	210(10)
	4	350(9)	340(10)	344(11)	352(13)	355(13)	345(9)
	5	373(17)	354(13)	363(22)	—	—	355(16)
	6	514(27)	506(23)	510(25)	522(29)	530(26)	528(20)
B_{3g}	1	149(9)	—	—	—	—	—
	2	190(8)	166(8)	170(11)	174(15)	175(11)	175(8)
	3	262(9)	255(11)	262(14)	270(10)	278(18)	281(10)
	4	341(10)	333(9)	342(13)	348(9)	352(16)	351(8)
	5	—	—	—	—	427(15)	428(19)

On the other hand, other modes have frequencies increasing with the atomic number increase. Physically, this could mean a dependence on the ionic radii or on the volume cell, which are both decreasing. In fact, the decreasing of the ionic radius led to changes in the unit cell volume which decreases on decreasing the *a* and *b* parameters, while the *c* parameter increases (table 1). As a consequence, the ionic interactions increase (the ions become closely packed), although bonding angles could also change due to the different behaviours of the lattice parameters. The effect on the Raman spectra should then be similar to the normal temperature behaviour, i.e., under cooling most of the phonon modes shift to higher frequencies. Then, we present in figure 4 the wavenumber variations with unit cell volume, for 19 of our 23 modes. Figure 4(a) (top) shows the modes that do not depend on the RE mass, while figure 4(b) (bottom) shows those that do depend on it. The symbols ●, ▲, ▽ and ◊ stand, respectively, for the modes of symmetries A_g, B_{1g}, B_{2g} and B_{3g}. The numbers for the modes correspond to those of table 3. The B_{1g} (No 1), B_{2g} (No 3) and B_{3g} (Nos 1 and 5) ones were not included in the figure because we do not have enough information to discern whether they belong to case (a) or (b).

We note first that ten of the eleven modes of figure 4(a) show the normal softening behaviour with the unit cell expansion. Only one mode, B_{2g} (No 2), presented an opposite abnormal hardening. This behaviour can be explained by the motions of the ions associated with this normal mode, which are more sensitive to the *c* axis contraction than to the cell volume expansion. Indeed, by using the projection operator, we have verified that for this mode, and only for this mode, the ions move preferentially along the *c*-axis [38].

Let us now analyse the results of figure 4(b). This figure shows that the frequencies of eight Raman modes are quite dependent on the RE mass. It is interesting to note that the site analysis

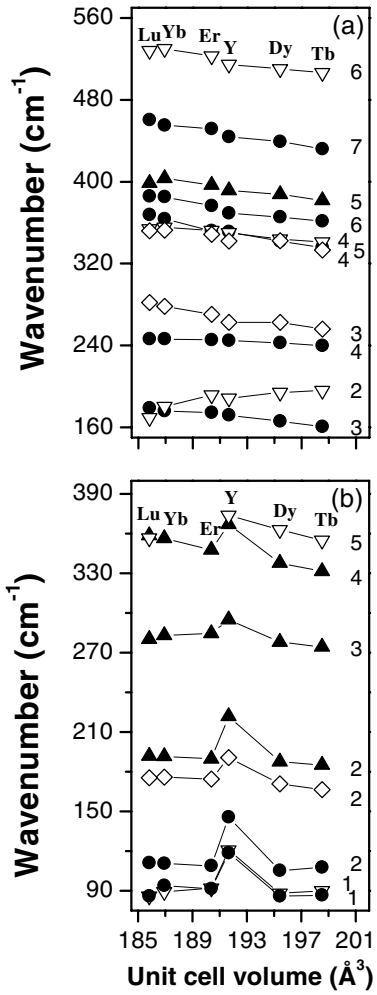

Figure 4. The variation of the Raman frequencies of YF_3 and isostructural LnF_3 lanthanides (Ln = Lu, Yb, Er, Dy, and Tb) as a function of the unit cell volume, for modes that (a) do not depend or (b) depend on the cationic mass. The numbers of the modes correspond to those of table 3. The symbols ●, ▲, ▽ and ◇ stand, respectively, for the modes of symmetries A_g, B_{1g}, B_{2g} and B_{3g}.

of table 2 gave for the RE ion the following even representation: $2A_g + B_{1g} + 2B_{2g} + B_{3g}$. Although all ions are involved in each irreducible representation (and we confirmed this by using the projection operators), we can see a relatively good correspondence between the number and type of modes whose polarizability changes depend on the RE ion (figure 4(b)) or on the fluorine ions (figure 4(a)) motion. It is worth noticing that the B_{1g} (No 4) and the B_{2g} (No 5) modes of figure 4(b) clearly depend on both the RE mass and unit cell volume.

The analysis above, within the framework of the physical property dependence on the unit cell parameters, can also be useful for explaining the differences in Raman profiles for the different crystals. Indeed, for the parallel polarizations as well as for the (ac) cross-polarized one the Raman intensities present an interesting variation with the particular RE ion. The important parameter here seems to be the orthorhombic elastic distortion ε, defined

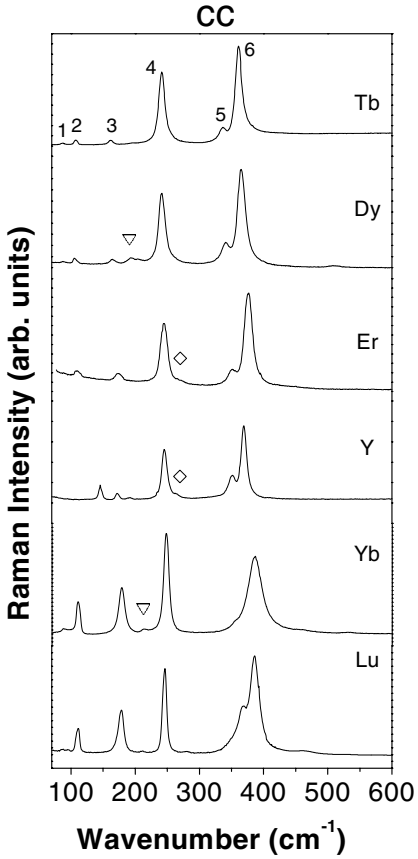

Figure 5. The totally symmetrical Raman spectra of REF_3 crystals with β-YF_3 structure, in the (cc) polarization. From the bottom to the top, the crystals are ranged in order of decreasing orthorhombic elastic distortion (see table 1). The peak leakages of B_{2g} and B_{3g} modes are indicated by the symbols $\triangledown$ and $\Diamond$, respectively.

in section 3. Then, we present in figure 5 the parallel-polarized Raman spectra in the (cc) configuration for all crystals studied here. The modes are numbered, in order to facilitate the comparison with the YF_3 modes. We recall that the A_g mode No 7 is not seen in this particular scattering geometry. From the bottom to the top, the spectra are presented for decreasing values of ε. We see a clear continuous evolution of the spectra with this parameter: the peak intensities of the A_g (No 2) and A_g (No 3) modes decrease from LuF_3 to TbF_3. These modes show the same behaviour in the other parallel configurations (not shown here). Now, we present in figure 6 the spectra of the cross-polarized (ac) geometry, for the RE crystals in the same order as in figure 5. The main feature here is the continuous weakening of the lower frequency B_{2g} (No 1) mode from LuF_3 to TbF_3, but we also observe the converse effect for the fourth B_{2g} band around 350 cm^{-1}, which becomes stronger.

We might now wonder why should the parameter ε drive the cross section (intensity) behaviour of some Raman peaks? The *tysonite* LaF_3 structure (D^4_{3d}) can be described as a face centred orthorhombic structure. For this structure, the ε parameter is obviously equal to zero. The *tysonite* structure is the most stable room temperature phase for LnF_3 crystals where the Ln atomic number is lower than 61. Besides, except for Ho, Dy and Tb, all the other LnF_3

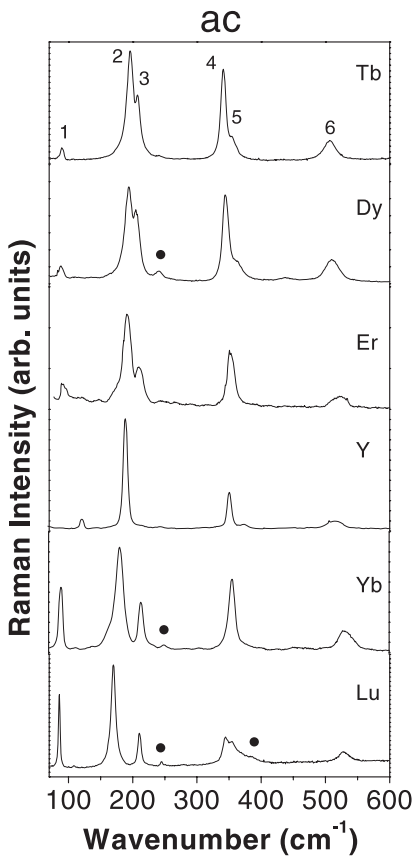

Figure 6. Raman spectra of REF_3 crystals with the β-YF_3 structure in the cross-polarized (*ac*) configuration. From the bottom to the top, the crystals are ranged in order of decreasing orthorhombic elastic distortion (see table 1). The symbol ● indicates peak leakage of A_g modes.

crystals (and also YF_3) also have a high temperature trigonal phase (which can be D^4_{3d} or D^3_{3d}, as described in section 1), which means that they undergo a ferroelastic phase transition, where one of the order parameters that vanish at the SPT should be the elastic distortion, as defined here. We should also point out that such a transition requires two independent order parameters, because of its reconstructive nature (it is necessary to consider both the D_{2h} and D_{3d} groups as derived from an actual or hypothetical common D_{6h} supergroup [39]). Thus, we interpret the decreasing of the Raman intensities of peaks in figures 5 and 6 as a pre-transitional-like effect in going from an orthorhombic D_{2h} to a trigonal D_{3d} point group. Then, we plot in figure 7 the normalized Raman intensities of the varying A_g modes No 2 and No 3 of our crystals in the (*cc*) polarization and the lower frequency B_{2g} mode, as functions of ε. The analogy to phase transitions appears clearly in this figure.

The Raman spectra of *tysonite* LnF_3 crystals show $5A_{1g}$ and $12E_g$ modes [22]. Four A_{1g} modes are located above 200 cm^{-1}, and correlate poorly with the A_g modes in our β-YF_3 crystals in the same spectral region. Although we do not expect a one-to-one correspondence between the totally symmetrical modes in the two structures, only one of the three low frequency modes could remain for decreasing ε. This could be the A_g (No 1) mode around 90 cm^{-1} (118 cm^{-1} for YF_3), which correlates well with the A_{1g} mode observed at 120 cm^{-1} in

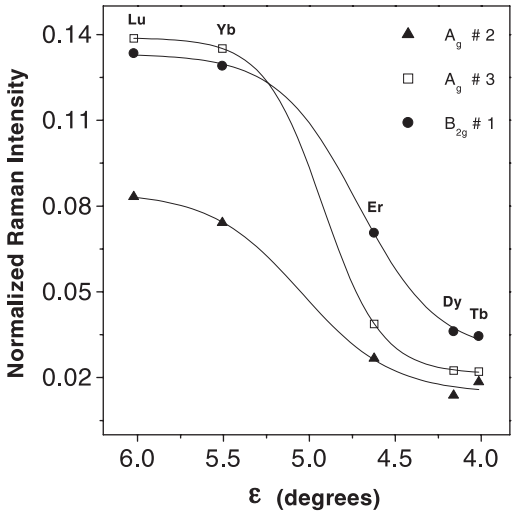

Figure 7. The variations of the Raman intensities of the lowest frequency A_g modes Nos 2 and 3 (in (cc) polarization) and B_{2g} mode No 1 of the LnF_3 crystals, as functions of the orthorhombic elastic distortion ε. The integrated intensity of each band has been normalized by the total area under all bands, for the corresponding spectra.

LaF_3 [22]. For the correspondence between our lower frequency B_{2g} mode (around 90 cm^{-1}) and the E_g modes of α-YF_3 the situation is more complicated, because of degeneracy and the mixture of symmetries. However, we also expect a reduction in the observed number of Raman-active modes from the β-YF_3 (24 modes) to the LaF_3 (17 modes) structure. Then, the vanishing of the B_{2g} mode shown in figures 6 and 7 is in agreement with this picture, although we should mention that LaF_3 exhibits one E_g band at 80 cm^{-1} [22].

5. Conclusions

Polarized Raman spectra of LnF_3 (Ln = Tb, Dy, Er, Yb and Lu) and YF_3 crystals with orthorhombic β-YF_3 structure were obtained for six different back-scattering configurations. 23 of the 24 modes of even parity predicted by factor group analysis were discerned. Three different parallel configurations were required to show all seven of the totally symmetric modes (A_g), indicating a dependence of the sample polarizability on the particular orientation of the Ln coordination polyhedra. By analysing the spectral evolutions with the RE mass and volume, we showed that some modes are more influenced by the motion of the RE ion, others by the fluorine ones, with a good correlation with group theory predictions. With increasing RE atomic number (ionic radii and volume decreasing) there is a general hardening of the modes associated with fluorine ion motion. The intensities of two low frequency A_g modes and of the lowest frequency B_{2g} mode depend strongly on the orthorhombic elastic distortion, tending to zero as this parameter decreases.

Acknowledgments

The authors are grateful to FAPEMIG, CAPES and CNPq for financial support and to Drs K Krambrock and C W A Paschoal for very useful discussions.

References

[1] Kaminskii A 1990 *Laser Crystals* (Berlin: Springer)
[2] Quarles G J, Esterowitz L, Rosenblat G M, Uhrin R and Belt R F 1992 *Proc. Adv. Solid State Lasers* **13** 306
[3] Petrov M V, Tkachuk A M and Feofilov P P 1981 *Izv. Akad. Nauk SSSR Ser. Fiz.* **45** 3
[4] Harmer A L, Linz A and Gabbe D R 1969 *J. Phys. C: Solid State Phys.* **30** 1483
[5] Meichenin D, Auzel F, Hubert S, Simoni E, Louis M and Gesland J Y 1994 *Electron. Lett.* **30** 1309
[6] Salaun S, Fornoni M T, Bulou A, Rousseau M, Simon P and Gesland J Y 1997 *J. Phys.: Condens. Matter* **9** 6941
[7] Salaun S, Fornoni M T, Bulou A, Rousseau M, Simon P and Gesland J Y 1997 *J. Phys.: Condens. Matter* **9** 6957
[8] Ayala A P, Guedes I, Freire P T C, Sasaki J M C, Melo F E A, Mendes Filho J and Gesland J Y 1999 *J. Phys.: Condens. Matter* **11** 5343
[9] Ayala A P, Paschoal C W A, Gesland J Y, Ellena J, Castellano E E and Moreira R L 2002 *J. Phys.: Condens. Matter* **14** 5485
[10] Kollia Z, Sarantopoulou E, Cefalas A C, Nicolaides C A, Naumov A K, Semashko V V, Abdulsabirov R Y, Korableva S L and Dubinskii M A 1995 *J. Opt. Soc. Am.* B **12** 782
[11] Zalkin A and Templeton D H 1953 *J. Am. Chem. Soc.* **75** 2453
[12] Cheetham A K and Norman N 1974 *Acta Chem. Scand.* A **28** 55
[13] Spedding F H and Henderson D C 1971 *J. Chem. Phys.* **54** 2476
[14] Sobolev B P and Fedorov P P 1973 *Sov. Phys.—Crystallogr.* **18** 392
[15] Sobolev B P, Ratnikova I D, Fedorov P P, Sinitsyn B V and Shanhkalamyan G S 1976 *Mater. Res. Bull.* **11** 999
[16] Sobolev B P, Fedorov P P, Seiranyan K B and Tkachenko N L 1976 *J. Solid State Chem.* **17** 201
[17] Greis O and Cader M S R 1985 *Thermochim. Acta* **87** 145
[18] Rotereau K, Gesland J Y, Daniel P and Bulou A 1993 *Mater. Res. Bull.* **28** 813
[19] Mansmann M 1964 *Z. Anorg. Allg. Chem.* **331** 98
[20] Mansmann M 1965 *Z. Kristallogr.* **122** 375
[21] Zalkin A, Templeton D H and Hopkins T E 1966 *Inorg. Chem.* **5** 1466
[22] Bauman R P and Porto S P S 1967 *Phys. Rev.* **161** 842
[23] Rotereau K, Daniel P and Gesland J Y 1998 *J. Phys. Chem. Solids* **59** 969
[24] Rotereau K, Daniel P, Desert A and Gesland J Y 1998 *J. Phys.: Condens. Matter* **10** 1431
[25] Guedes K J, Krambrock K and Gesland J Y 1999 *J. Phys.: Condens. Matter* **11** 7211
[26] Guedes K J, Krambrock K and Gesland J Y 2001 *J. Phys. Chem. Solids* **62** 485
[27] Misra S K, Mikolalczak P and Lewis N R 1981 *Phys. Rev.* B **24** 3729
[28] Misra S K, Mikolalczak P and Korczak S 1981 *J. Chem. Phys.* **74** 922
[29] Wilmarth W R, Begun G M, Nave S E and Peterson J R 1988 *J. Chem. Phys.* **89** 711
[30] Kraus J, Görlitz W, Hirsch M, Roth R and Schaack G 1989 *Z. Phys.* B **74** 247
[31] Thoma R E, Weaver C F, Friedman H A, Insley H, Harris L A and Yakel H A 1961 *J. Phys. Chem.* **65** 1096
[32] Porto S P S and Scott J F 1967 *Phys. Rev.* **157** 716
[33] Hayes W and Loudon R 1978 *Scattering of Light by Crystals* (New York: Wiley)
[34] Shannon R D 1976 *Acta Crystallogr.* A **32** 751
[35] Rousseau D L, Bauman R P and Porto S P S 1981 *J. Raman Spectrosc.* **10** 253
[36] Wyckoff R G 1965 *Crystal Structures* (New York: Wiley)
[37] Turrel G 1972 *Infrared and Raman Spectra of Crystals* (London: Academic) pp 164–9
[38] Lage M M, unpublished results
[39] Toledano J C and Toledano P 1987 *The Landau Theory of Phase Transitions* (Singapore: World Scientific)